The Humidity and Temperature Sensitivity of Clear-Air Radars in the Convective Boundary Layer

C. W. FAIRALL

NOAA Wave Propagation Laboratory, Boulder, Colorado

(Manuscript received 18 September 1990, in final form 5 February 1991)

ABSTRACT

A top-down/bottom-up diffusion model is used to evaluate the relative contributions of humidity, temperature, and their cross correlation to the radar refractive index structure function paramer C_n^2 in the cloud-free, convective planetary boundary layer (PBL). Profiles of C_n^2 can be measured continuously in the clear air with Doppler radars. Extraction of information about PBL dynamical parameters is more straightforward if C_n^2 is dominated by either moisture (C_q^2) or temperature (C_T^2). In the lower part of the PBL the surface Bowen ratio β_0 determines this dominance. In the upper part of the PBL the inversion Bowen ratio β_i is the primary determining factor. The model suggests that humidity accounts for at least 75% of C_n^2 over tropical and midlatitude oceans. Polar oceans, where β_0 often exceeds 0.5, may not be dominated by either temperature or moisture. Over land β_0 can easily vary from 0.1 to 10. Geographical regions with $\beta_0 < 0.3$ will be dominated by C_q^2 in the lower PBL; regions with $\beta_0 > 5$ will be dominated by C_T^2. Even for large values of β_0, the upper part of the PBL will often be dominated by humidity.

1. Introduction

The development of Doppler wind profiling radars (profilers) has greatly expanded opportunities for atmospheric monitoring and research (Balsley and Gage 1982). These systems are often referred to as "clear-air" radars because their operation does not require the presence of clouds, precipitation, or insects; rather they are capable of receiving returns from refractive index inhomogeneities, which are almost always present, in varying degrees of intensity in the turbulent troposphere and stratosphere. The relative sensitivity of a given radar to the various scattering mechanisms aforementioned is primarily a function of wavelength (Chadwick and Gossard 1986; Gossard 1990), with refractive turbulence dominating at longer wavelengths.

The introduction of higher frequency (915 MHz or 33-cm wavelength) profilers (Strauch et al. 1984; Ecklund et al. 1988) with much shorter pulses now permits measurements with vertical resolution approaching 50 m. Such systems have great potential for boundary-layer research and applications. The profilers provide information not only on the wind profile (from the Doppler shift), but also on the refractive index structure function parameter C_n^2 (from the intensity of the received backscattered signal). The refractive index structure function parameter is related to the micrometeorological structure function parameters for temperature C_T^2, humidity C_q^2, and the temperature–humidity correlation structure function parameter C_{Tq} (Wesely 1976). Thus, profilers are capable of providing information about small-scale turbulence in the planetary boundary layer (PBL). Such information is a useful diagnostic of PBL dynamics (Fairall 1987a), is relevant to electromagnetic and acoustic propagation in the boundary layer, and may be useful in computing more representative areal averages of surface scalar fluxes (Wyngaard 1990) than is possible with a point measurement from a tower.

Because C_n^2 involves contributions from C_T^2, C_q^2, and C_{Tq}, a given radar measurement does not unambiguously determine any one of these parameters except under special circumstances. For example, in the marine PBL (MPBL) the humidity term often dominates (Burk 1980); it is expected that temperature dominates over desert regions. In this paper we will examine the relative dominance of temperature and humidity in the convective PBL using the top-down and bottom-up diffusion scaling developed by Wyngaard and Brost (1984) and extended to structure function parameters by Fairall (1987b). The model is applicable to cloud-free, horizontally homogeneous, and stationary conditions. This model obeys Monin–Obukhov similarity (Wyngaard et al. 1971) near the surface, but allows the entrainment of dry, warm air from above the PBL to influence the structure function profiles. The entrainment effect is particularly important in the upper part of the PBL. Entrainment is often characterized by the entrainment velocity W_e, which describes at what rate the depth of the boundary layer increases due

Corresponding author address: Dr. C. W. Fairall, NOAA, Wave Propagation Laboratory, 325 Broadway, Boulder, CO 80303-3328.

to turbulent engulfment of nonturbulent air above the PBL.

The top-down/bottom-up formulation is applicable from the surface layer up to, but not including, the inversion that caps the mixed layer. Burk (1981) has already examined the moisture–temperature contributions to C_n^2 in the inversion region using the Wyngaard–LeMone scaling approach. Since the humidity term often dominates in the PBL, we will express C_n^2 as proportional to C_q^2 with a term α_r^2, which represents deviations from pure moisture contributions to C_n^2 (Wesely 1976). We will show that shape of the α_r^2 profile can be characterized in terms of three basic dimensionless scaling variables: the surface Bowen ratio β_0, the inversion Bowen ratio β_i, and the ratio of the surface to the inversion (i.e., entrainment) temperature fluxes R_T.

2. Background

a. Turbulence parameters

Consider some atmospheric variable $X(r)$ as a function of location r. The structure function $D_x(d)$ of X is defined by (Panofsky and Dutton 1984)

$$D_x(d) = \overline{[X(r+d) - X(r)]^2} \tag{1}$$

where d denotes a separation distance and the overbar denotes an ensemble average. The atmospheric variables of interest here are temperature T, specific humidity q, and refractive index n. At small size scales, atmospheric turbulence tends to be isotropic, and D_x has a 2/3 power dependence on separation until the scales become so small that the fluctuations are directly influenced by dissipation. In this inertial subrange of isotropic turbulence, the structure function parameter is defined as

$$C_x^2 = D_x(d)/d^{2/3}, \tag{2}$$

which is independent of d.

The temperature–humidity cross-correlation structure function parameter is also defined as

$$C_{Tq} = \overline{[(T(r+d) - T(r)][q(r+d) - q(r)]}/d^{2/3}. \tag{3}$$

The small-scale T–q correlation coefficient r_{Tq} is defined (Wesely 1976) as

$$r_{Tq} = C_{Tq}/(C_T C_q). \tag{4}$$

In the inertial subrange of isotropic turbulence the fluctuations in spatial coordinates are characterized by a one-dimensional variance spectral density $S_x(k)$; correlations of temperature–humidity fluctuations are characterized by the T–q cospectrum $S_{Tq}(k)$:

$$S_x(k) = 0.25 C_x^2 k^{-5/3} \tag{5a}$$

$$S_{Tq}(k) = 0.25 C_{Tq} k^{-5/3} \tag{5b}$$

where k is the wavenumber magnitude and 0.25 is a mathematical constant (Wyngaard et al. 1971). The variances of X, σ_x^2, and the T–q covariance $\overline{\theta' q'}$ are obtained from the integral of the respective spectra over all wavenumbers (the primes denote fluctuations). The use of the potential temperature symbol θ here is traditional and allows us a notational distinction for a second correlation variable. Note that (Wyngaard et al. 1978) a large-scale correlation coefficient $r_{\theta q}$ can be defined as

$$r_{\theta q} = \overline{\theta' q'}/\sigma_T \sigma_q, \tag{6}$$

which is distinct from r_{Tq} because (5a) and (5b) describe a restricted portion of the wavenumber spectra, whereas (6) is in terms of integrals over the entire spectrum.

b. Radar C_n^2

For radar half-wavelength $\lambda/2$ of size scale within the inertial subrange of isotropic turbulence, the radar reflectivity or scattering cross section per unit volume η is given by (Ottersten 1969) as

$$\eta = 0.38 C_n^2 \lambda^{-1/3}. \tag{7}$$

The radio refractive index of air is a function of temperature, humidity, and pressure. Fluctuations in the refractive index can be expressed as a linear combination of fluctuations of temperature and humidity [pressure fluctuations can generally be ignored (Burk 1980)] and used in (1) and (2) to obtain an expression for C_n^2 in terms of the scalar structure function parameters (Wesely 1976):

$$C_n^2 = (6 \times 10^{-4} P/T^2)^2 C_q^2 \alpha_r^2 \tag{8}$$

where C_q^2 is given in $(\text{g kg}^{-1})^2\ \text{m}^{-2/3}$ units, pressure in millibars (mb), temperature in kelvin (K), and $\alpha_r^2 - 1$ gives the deviations from pure moisture dominated C_n^2. If the mean-moisture variable q is expressed in grams per kilogram, then

$$\alpha_r^2 = 1 - 2a r_{Tq} C_T/C_q + a^2 C_T^2/C_q^2 \tag{9}$$

where (Gossard 1990)

$$a = 0.13(1 + 15.4\bar{q}/\bar{T}). \tag{10}$$

3. Top-down/bottom-up diffusion model

a. Dimensionless structure functions

The analysis presented in this paper is concerned with the atmospheric boundary layer. A scaling model that is applicable for the unstable, cloud-free boundary layer capped with an inversion at a height z_i will be used. An unstable PBL is typical over land during the daytime and most of the time over the ocean. The model is not applicable when PBL clouds are present in significant amounts (see section 6).

The profiles of C_q^2, C_T^2, and C_{Tq} in the convective

boundary layer are parameterized (Fairall 1984; Fairall 1987b) using the top-down and bottom-up diffusion scaling approach (Wyngaard and Brost 1984). The structure function profiles are represented by similarity forms

$$C_q^2 z_i^{2/3}/Q_*^2 = f_q(\xi) \quad (11a)$$

$$C_T^2 z_i^{2/3}/\Theta_*^2 = f_T(\xi) \quad (11b)$$

$$C_{Tq} z_i^{2/3}/\Theta_* Q_* = f_{Tq}(\xi) \quad (11c)$$

where the $f(\xi)$ functions are the dimensionless structure function parameters, $\xi = z/z_i$ the dimensionless height, and Θ_* and Q_* are the standard temperature and moisture convective scaling parameters (Moeng and Wyngaard 1984) defined in terms of the convective scaling velocity W_* and the turbulent scalar surface fluxes

$$\Theta_* = \overline{w'T'_0}/W_* \quad (12a)$$

$$Q_* = \overline{w'q'_0}/W_*. \quad (12b)$$

In these equations the "0" subscript indicates a surface value.

The dimensionless structure function parameters are represented in top-down/bottom-up form (Moeng and Wyngaard 1984; Fairall 1987b)

$$f_q(\xi) = h_b(\xi) + R_q h_{tb}(\xi) + R_q^2 h_t(\xi) \quad (13a)$$

$$f_{Tq}(\xi) = h_b(\xi) + 0.5(R_q + R_T)h_{tb}(\xi) + R_q R_T h_t(\xi) \quad (13b)$$

$$f_T(\xi) = h_b(\xi) + R_T h_{tb}(\xi) + R_T^2 h_t(\xi). \quad (13c)$$

The $h(\xi)$ functions are empirically derived from large eddy simulation (LES) results (see following). The subscripts refer to bottom-up (b), top-down (t), and mixed (tb) diffusion processes. The parameters R_T and R_q are the ratios of the inversion-layer fluxes (i.e., the fluxes at the top of the boundary layer) to their surface values. Following Lilly (1968), Wyngaard and LeMone (1980), and Wyngaard (1990), this analysis will assume that the inversion flux can be approximated by

$$\overline{w'x'_i} = -W_e \Delta X \quad (14)$$

where ΔX is the increase (jump) in the mean of X across the inversion region.

To compute the structure function profiles, the forms of the $h(\xi)$ functions and specification of R_T and R_q are needed. For the classic cloud-free, convectively driven PBL, $R_T \approx -0.2$ (Tennekes and Driedonks 1981). To account for the effects of surface-generated shear turbulence, Fairall (1984) suggested a modification to this simple parameterization

$$R_{Tv} = -0.2[1 + 3.2(-L/z_i)] \quad (15)$$

where L is the Monin–Obukhov stability length and Tv denotes the virtual temperature. From the definition of virtual temperature, a relationship between R_T and R_{Tv} can be easily obtained by

$$R_T = R_{Tv}(1 + 0.07/\beta_0)(1 + 0.07/\beta_i)^{-1} \quad (16)$$

where β_0 and β_i are the surface and inversion Bowen ratios.

Because inversion wind shear and very small amounts of clouds can significantly increase entrainment rates, R_{Tv} will be treated as an externally specified parameter and R_q will be computed as

$$R_q = \overline{w'q'_i}/\overline{w'q'_0} = -W_e \Delta q/W_* Q_* = (\beta_0/\beta_i)R_T \quad (17)$$

where β_i is given by

$$\beta_i = c_p \Delta\theta/(L_e \Delta q), \quad (18)$$

$L_e/c_p = 2.5$ is the ratio of the heat of vaporization of water (using g kg^{-1} moisture units) to the specific heat of air, $\Delta\theta$ is the jump in potential temperature across the inversion, and Δq is the jump in specific humidity (usually negative).

Because latent and sensible heat fluxes provide a natural way to compare the moisture and temperature turbulence, (17) will be used to eliminate R_q and express the structure function profiles in terms of R_T and the ratio β_0/β_i:

$$f_q(\xi) = h_b(\xi) + (\beta_0/\beta_i)R_T h_{tb}(\xi) + (\beta_0/\beta_i)^2 R_T^2 h_t(\xi) \quad (19a)$$

$$f_{Tq}(\xi) = h_b(\xi) + 0.5(1 + \beta_0/\beta_i)R_T h_{tb}(\xi) + (\beta_0/\beta_i)R_T^2 h_t(\xi) \quad (19b)$$

$$f_T(\xi) = h_b(\xi) + R_T h_{tb}(\xi) + R_T^2 h_t(\xi). \quad (19c)$$

Following (8) and (11) the normalized form of the refractive index structure function parameter is obtained by

$$C_n^2 z_i^{2/3}(6 \times 10^{-4} P/T^2)^{-2} = Q_*^2 f_q(\xi)\alpha_r^2 \quad (20)$$

where

$$\alpha_r^2 = [1 - 5a\beta_0 f_{Tq}(\xi)/f_q(\xi) + (2.5a\beta_0)^2 f_T(\xi)/f_q(\xi)]. \quad (21)$$

The factors of 5 and 2.5 in (21) come from direct substitution of L_e/c_p.

The empirical dimensionless profile functions $h_x(\xi)$ used here were determined from the dimensionless variance functions $g_x(\xi)$ and the turbulent dissipation time scales $\tau_x(\xi)$ in the manner described by Fairall (1987b). The subscript x is used here to denote the fact that these computations are carried separately for the bottom-up ($x = b$), top-down ($x = t$), and cross-term functions ($x = tb$). The dimensionless variance profiles have the same top-down/bottom-up form as in (11) and (19). For example, the dimensionless profile of potential temperature variance σ_θ^2 is

$$\sigma_\theta^2/\theta_*^2 = g_b(\xi) + R_T g_{tb}(\xi) + R_T^2 g_t(\xi), \quad (22)$$

and there are similar expressions for σ_q^2 and $\overline{\theta' q'}$. The $h(\xi)$ functions are obtained from the simple expression

$$h_x(\xi) = 2.3 g_x(\xi)/\tau_x(\xi). \quad (23)$$

This study used the new results for $g_x(\xi)$ and $\tau_x(\xi)$ from more recent top-down/bottom-up diffusion LES computations (Moeng and Wyngaard 1989, see their Figs. 12 and 22):

$$h_b(\xi) = 10(-z_i/L)^{2/3}[\xi(1 - 7z/L)]^{-2/3} \quad (24a)$$

$$h_{tb}(\xi) = 8(1 - 0.8\xi) \quad (24b)$$

$$h_t(\xi) = 10(1 - \xi)^{-2/3}(2 - \xi)^{-1}. \quad (24c)$$

The original functions were based on LES results computed on a grid with $(40)^3$ points. The more recent work uses a grid of $(96)^3$ points and corrects some of the deficiencies of the earlier study, such as insufficient temperature variance in the mixed layer. Note that to determine the profile of α_T^2 the dimensionless parameters R_T, β_0, β_i, and z_i/L must be specified. In the free convection limit, (z_i/L) drops out and (24a) reduces to the classic result $h_b(\xi) = 2.7\xi^{-4/3}$. Since the lowest measurement height of even the high resolution profilers is usually above the transition to the free convection regime, the z_i/L dependence will be ignored in the examples used in this paper.

b. Scaling limits

Before examining specific PBL conditions, it is of interest to look at the asymptotic limits predicted by the scaling model. There are two obvious scaling limits: 1) entrainment negligible ($R_{Tv} \approx 0$) and 2) entrainment dominant ($-R_{Tv} \gg 1$). For typical values of the scaling parameters, h_b will dominate (19) in the lower part of the PBL and h_t will dominate in the upper part of the PBL (see Druilhet et al. 1983 for an atypical example). Thus, even if R_{Tv} does not meet these extreme limits, the entrainment negligible limit will be useful to describe the near-surface region of the PBL and the entrainment dominated limit will describe the near-inversion region of the PBL. If the first condition is applied, then the dimensionless functions (19) become $h_b(\xi)$ and it is found that

$$C_n^2 z_i^{2/3}(6 \times 10^{-4} P/T^2)^{-2} = Q_*^2 h_b(\xi)\alpha_r^2 \quad (25)$$

where $\alpha_r = (1 - 2.5a\beta_0)$. This result implies that $|r_{Tq}| = 1$, which is consistent with pure surface-layer similarity (Hill 1989). If $q = 8$ g kg^{-1} and $T = 300$ K are used, then we find $\alpha_r = (1 - 0.46\beta_0)$ as is also given by Burk (1980). For the entrainment-dominated condition, we find

$$C_n^2 z_i^{2/3}(6 \times 10^{-4} P/T^2)^{-2} = (W_e/W_*)^2 \Delta q^2 h_t(\xi)\alpha_r^2 \quad (26)$$

where now $\alpha_r = (1 - 2.5a\beta_i)$ and clearly it is the characteristics of the inversion that determine the relative importance of moisture and temperature. Remember that this latter result is not valid within the inversion region. According to the Wyngaard–LeMone model of structure functions in the inversion (Fairall 1984), the temperature fluctuations are considerably suppressed relative to the moisture fluctuations: $C_T^2/C_q^2 \approx (\Delta\theta/\Delta q)^2/7$. Therefore, within the inversion it is expected that $\alpha_r = (1 - 2.5a\beta_i/\sqrt{7})$.

c. Comparisons with atmospheric measurements

Fairall (1987b) compared the original form of this model with a wide variety of aircraft-measured profiles of C_T^2 and C_q^2 with reasonably good results. An under prediction of C_T^2 in the mixed layer that is observed in the aircraft data for some cases has been considerably improved with the new LES results; however, some disagreement remains. The comparisons with C_q^2 remain very good. For determination of α_T^2 profiles, the C_T^2 disagreement is relatively less important. For $-\beta_i < 4$ Burk (1981) showed that the second term in (9) is at least five times larger than the third term in the inversion, where $r_{Tq} \approx -1$. Near the surface, a similar conclusion can be drawn for $\beta_0 < 4$ if $r_{Tq} \approx 1$. Thus, for typical atmospheric conditions the C_{Tq} term is more important than the C_T^2 term in determining the relative importance of moisture in radar-measured C_n^2 in the PBL. Regions where r_{Tq} is small are likely to have negligible temperature contributions.

Unfortunately, measurements of the profile of C_{Tq} or $r_{Tq} = C_{Tq}/(C_T C_q)$ in the convective PBL are not available in the literature. Figure 1 shows a comparison of the model for r_{Tq} with aircraft measurements of the θ–q correlation $\overline{\theta' q'}/(\sigma_q \sigma_\theta)$ made during the AMTEX program (Wyngaard et al. 1978). Model curves are given for $R_q = 0.5$, 1.0, and 1.5, which are expected to bracket the AMTEX conditions. The agreement here is poor, but is consistent with Wyngaard et al.'s (1978) finding that the θ–q correlation has a different behavior than the θ–q dissipation. They give an example of a θ–q cospectrum from $\xi = 0.5$, which is negative at low frequencies and positive at high frequencies and state that r_{Tq} and $r_{\theta q}$ would cross zero at the same height "if θ and q were correlated in the same sense at all frequencies."

The difference in the $r_{\theta q}$ and r_{Tq} within the top-down/bottom-up formalism is due to the three different time scales (bottom-up, top-down, and cross term) that relate the dissipations to the variances and covariances [see earlier discussion associated with Eqs. (22) and (23)]. This can be confirmed by comparing the AMTEX data with the top-down/bottom-up diffusion model for the θ–q correlation [i.e., use the $g_x(\xi)$ functions], which is shown in Fig. 1b. Here the agreement is clearly better than Fig. 1a. Note that r_{Tq} crosses zero at a higher point in the mixed layer than the θ–q cor-

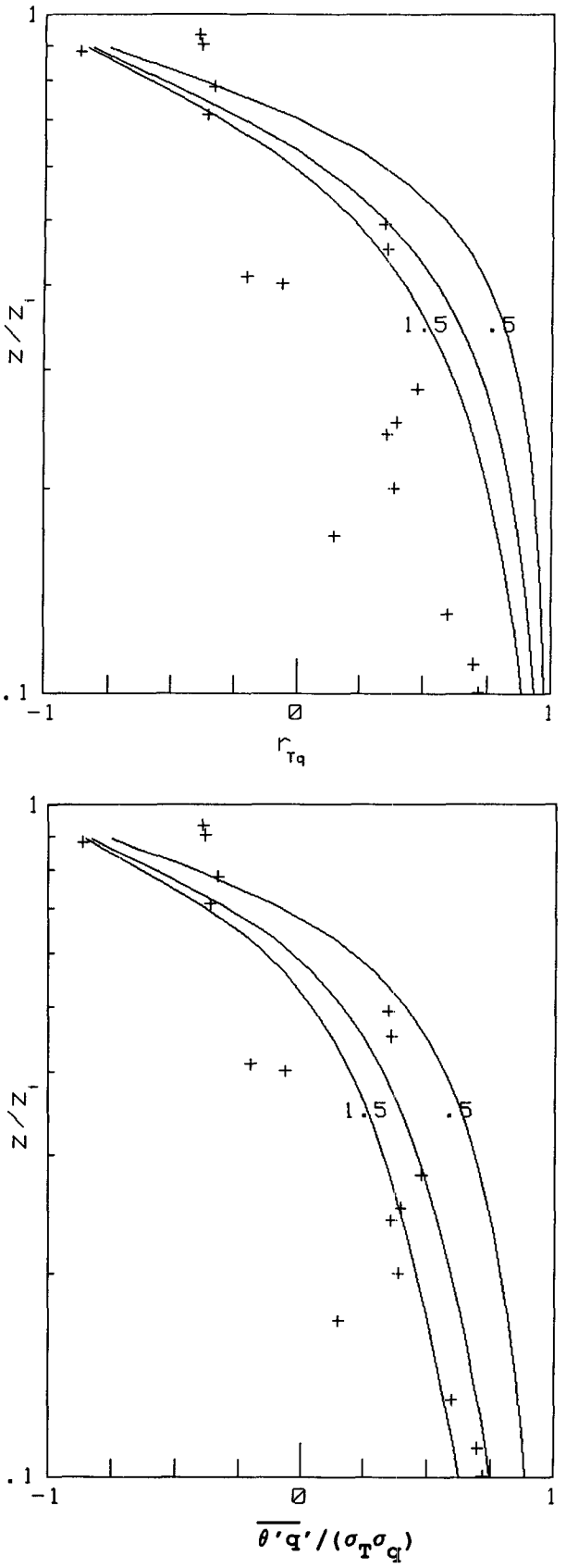

relation, which is consistent with Wyngaard et al.'s (1978) analysis.

4. Surface Bowen ratios

Near the surface the sensible and latent heat fluxes are proportional to the vertical gradients of potential temperature and specific humidity. Using arguments about the gradients, Priestly and Taylor (1972) expressed the Bowen ratio as

$$\beta_0 = [\gamma + (1 - \alpha)s]/(\alpha s) \tag{27}$$

where $\gamma = c_p/L_e$ and s is the temperature derivative of the water-vapor saturation specific humidity $q_s(T)$. The value s is computed from the Clausius–Claperyon relation;

$$s = \partial q_s(T)/\partial T = (\epsilon L_e/RT^2)q_s(T), \tag{28}$$

where $\epsilon = 0.622$ and R is the gas constant for air. Here α is an empirical coefficient (not to be confused with α_r associated with radar temperature–humidity sensitivity) defined as

$$\alpha = \frac{(s + \gamma)}{s} \frac{\overline{w'q'_0}}{(\overline{w'q'_0} + \gamma \overline{w'T'_0})}. \tag{29}$$

Priestly and Taylor (1972) suggest $\alpha \approx 1.25$ over saturated land surfaces and over the ocean in "advection-free" conditions. Using this value of α in (27), Priestly and Taylor (1972) show that the temperature dependence of s leads to a Bowen ratio that decreases from about 0.45 at a temperature of 283 K to 0.0 at 308 K.

Because the ocean is not generally nonadvective, α is not a universal constant. However, the surface fluxes over the ocean can be expressed with conventional bulk transfer relations (Smith 1988)

$$\overline{w'T'_0} = c_h \bar{u}\, \delta\theta \tag{30a}$$

$$\overline{w'q'_0} = c_e \bar{u}\, \delta q \tag{30b}$$

where u represents the wind speed measured at 10 m above the sea surface, c_h and c_e are the bulk transfer coefficients ($\approx$0.001), $\delta\theta$ the sea–air potential temperature difference, and δq the sea–air specific humidity difference given by

$$\delta q = q_s(\bar{T}_s) - \bar{S} q_s(\bar{T}). \tag{31}$$

Here T_s is the surface temperature, T is the air temperature, q_s is the saturation specific humidity at the indicated temperature, and S is the saturation ratio. The advantage of this approach is that there is a vast

FIG. 1. Normalized temperature–humidity correlations in the convective PBL versus normalized height $\xi = z/z_i$ (log scale). The solid lines are the top-down/bottom-up diffusion model with $\beta_0 = 0.35$, $R_T = -0.2$, and $R_q = 0.5$, 1.0 and 1.5. The plus symbols are for $\overline{\theta'q'}/(\sigma_\theta \sigma_q)$ measured during AMTEX (Wyngaard et al. 1978). (a) Model results for $r_{Tq} = C_{Tq}/(C_T C_q)$ and (b) model results for $\overline{\theta'q'}/(\sigma_\theta \sigma_q)$.

TABLE 1. Typical marine meteorological conditions, surface Bowen ratios, and resultant implications for near-surface α_T^2 for three climate regimes.

Climate regime	T (K)	q (g kg^{-1})	β_0	$2.5a$	α_T^2
Tropical	303	20	0.1	0.65	0.87
Midlatitude	288	8	0.25	0.46	0.78
Polar	270	2	1.0	0.36	0.41

global ocean database of measurements of the bulk quantities.

If it is assumed that $\delta\theta \approx \delta T = T_s - T$ and that the moisture and temperature transfer coefficients are the same, then the surface Bowen ratio may be expressed as

$$\beta_0 = \gamma\delta T/[q_s(\bar{T} + \delta T) - \bar{S}q_s(\bar{T})]. \quad (32)$$

Note that now the empirical coefficients cancel out of the relationship. Using (28) to expand $q_s(T + \delta T)$,

$$\beta_0 = \gamma\delta T/[q_s(\bar{T})(1 - S + \epsilon L_e\delta T/R\bar{T}^2)] \quad (33)$$

is obtained. For $\gamma = 0.4$ and $T \approx 290$ K, the surface Bowen ratio over the ocean will be approximately given by

$$\beta_0 = 0.4\delta T/[(1 - \bar{S}) + 0.06\delta T]q_s(\bar{T}). \quad (34)$$

Typical midlatitude marine values are $S \approx 0.8$ and $\delta T \approx 1$ K (Hsiung 1986). Since β_0 is inversely proportional to $q_s(T)$, β_0 will be much smaller in the tropics than in the polar ocean regions for the same value of δT. Assuming $S = 0.8$ and $\delta T = 1$ K, (34) gives $\beta_0 = 0.06$ for $T = 303$ K and $\beta_0 = 0.4$ for $T = 270$ K. However, the average δT tends to be larger than 1 K in polar regions, where the annual average β_0 can be as large as 2.0 (Hakkinen and Cavalieri 1989). Table 1 gives some average values of β_0 and α_T^2 for three marine climate regimes. Of course the values of S and δT are subject to considerable variability on synoptic time scales. There are also systematic variations both seasonally and with geographic location, but these tend to be much smaller than variations observed over land.

Surface Bowen ratios over land are much more variable than over oceans: seasonally, geographically, and even diurnally. Because we are discussing the convective PBL, we are primarily concerned with daytime conditions over land. Since solar radiation is absorbed at the surface over land, the latent and sensible heat fluxes tend to be determined by the balance of net radiation and heat flux into the ground. Thus, the Bowen ratio is closely coupled to the soil moisture content and partially controlled by plant physiology (Priestly and Taylor 1972; Carlson 1986; Stull 1988). Furthermore, land conditions vary from deserts where β_0 can exceed 10 to rain forests and swamps where β_0 can be as small that for oceans, with a wide variety of surface conditions in between. For example, Prentice (1990) lists 30 different climate zones used to characterize vegetation in general circulation models. This situation is obviously too complex to summarize in a manner analogous to Table 1. However, a value of β_0 between 0.5 and 2.0 will be found in a significant fraction of daytime, over land conditions.

5. Examples

In the convective limit, α_T^2 depends on R_T, β_0, and β_i: the scalar structure functions and r_{Tq} are slightly simpler because the Bowen ratios enter the expressions as β_0/β_i. The basic expressions are contained in (19), (20), (21), and (24). These equations are fairly simple and can be programed on a desktop computer in less than an hour. Thus, there is no practical reason to present a set of complicated figures that explore all possible permutations of the basic parameters. Examples will be given that illustrate the behavior of the PBL profiles for three common cases: 1) a marine subsidence regime such as the coast of California, 2) a marine trade wind regime such as the Bahamas, and 3) a moderately dry central United States regime such as the Great Plains. Case 3 is only moderately drier than the mixed forest and agricultural land of central Pennsylvania, where β_0 is typically on the order of 0.5 (Rabadi 1990). The parameters we have chosen for these regimes are given in Table 2. The marine cases are median examples taken from the data given in Fairall (1984); the overland case is chosen for Colorado on a mostly cloud-free summer afternoon. A "Central Plains" Bowen ratio on the order of 1 is reasonable for Colorado. Kohsiek (1982) found daytime β_0 values between 0.4 and 20 with a median of 2 from a series of measurements near Boulder, Colorado, between January and March. Priestley and Hill (1985) found β_0 between 1.5 and 6.8 with a median of 3 for "very dry" conditions in August at the same site. Measure-

TABLE 2. Typical marine meteorological conditions, surface Bowen ratios, and inversion-layer characteristics for three sample climate regimes.

Climate regime	T (K)	q (g kg^{-1})	β_0	z_i (km)	$\Delta\theta$ (K)	Δq (g kg^{-1})	β_i
California coastal	288	8	0.25	0.50	8	−4	−0.8
Trade wind	298	12	0.25	1.5	2.5	−5	−0.2
Central Plains	298	8	1.0	2.0	2.5	−2.5	−0.4

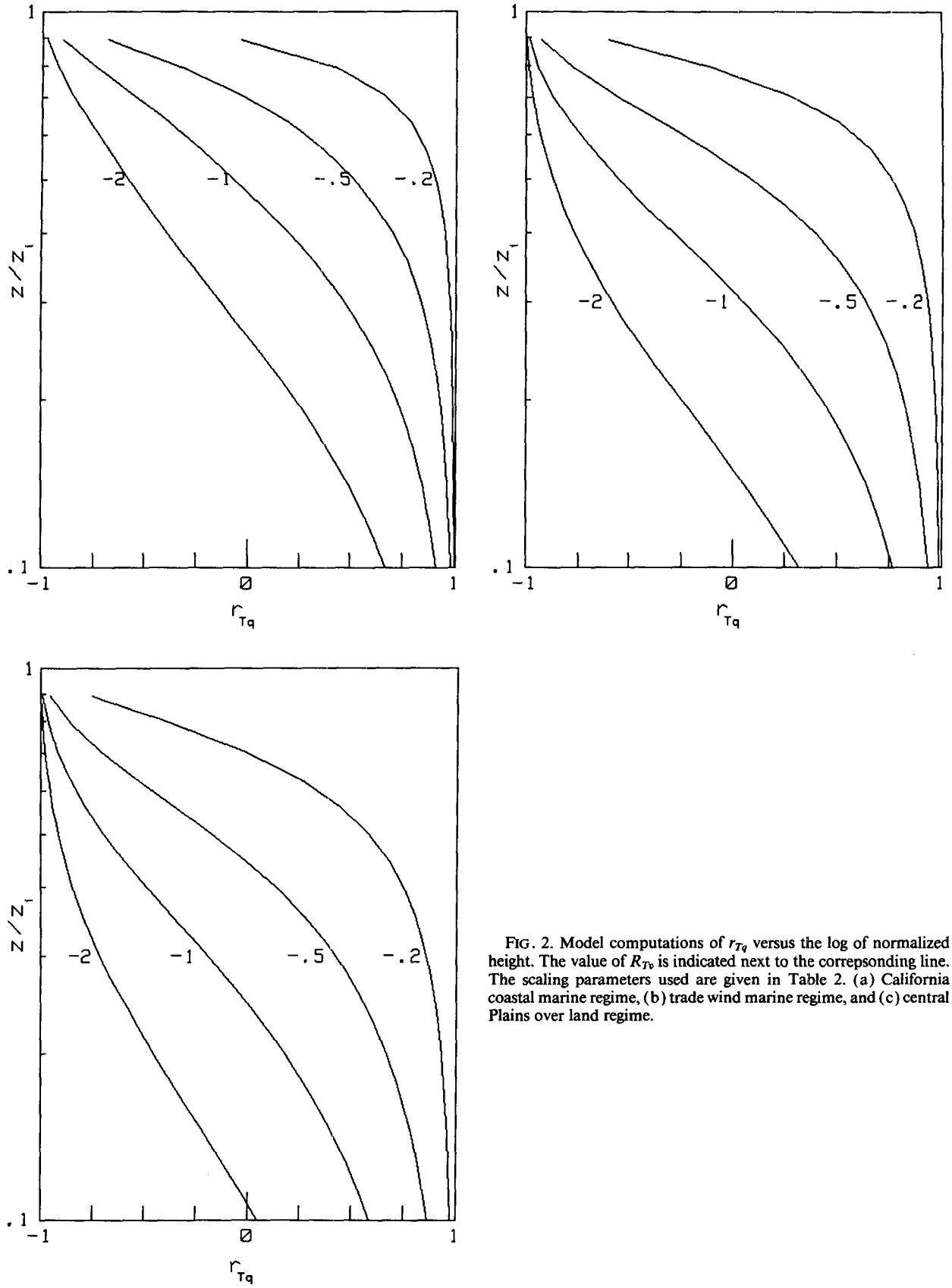

FIG. 2. Model computations of r_{Tq} versus the log of normalized height. The value of R_{Tv} is indicated next to the correpsonding line. The scaling parameters used are given in Table 2. (a) California coastal marine regime, (b) trade wind marine regime, and (c) central Plains over land regime.

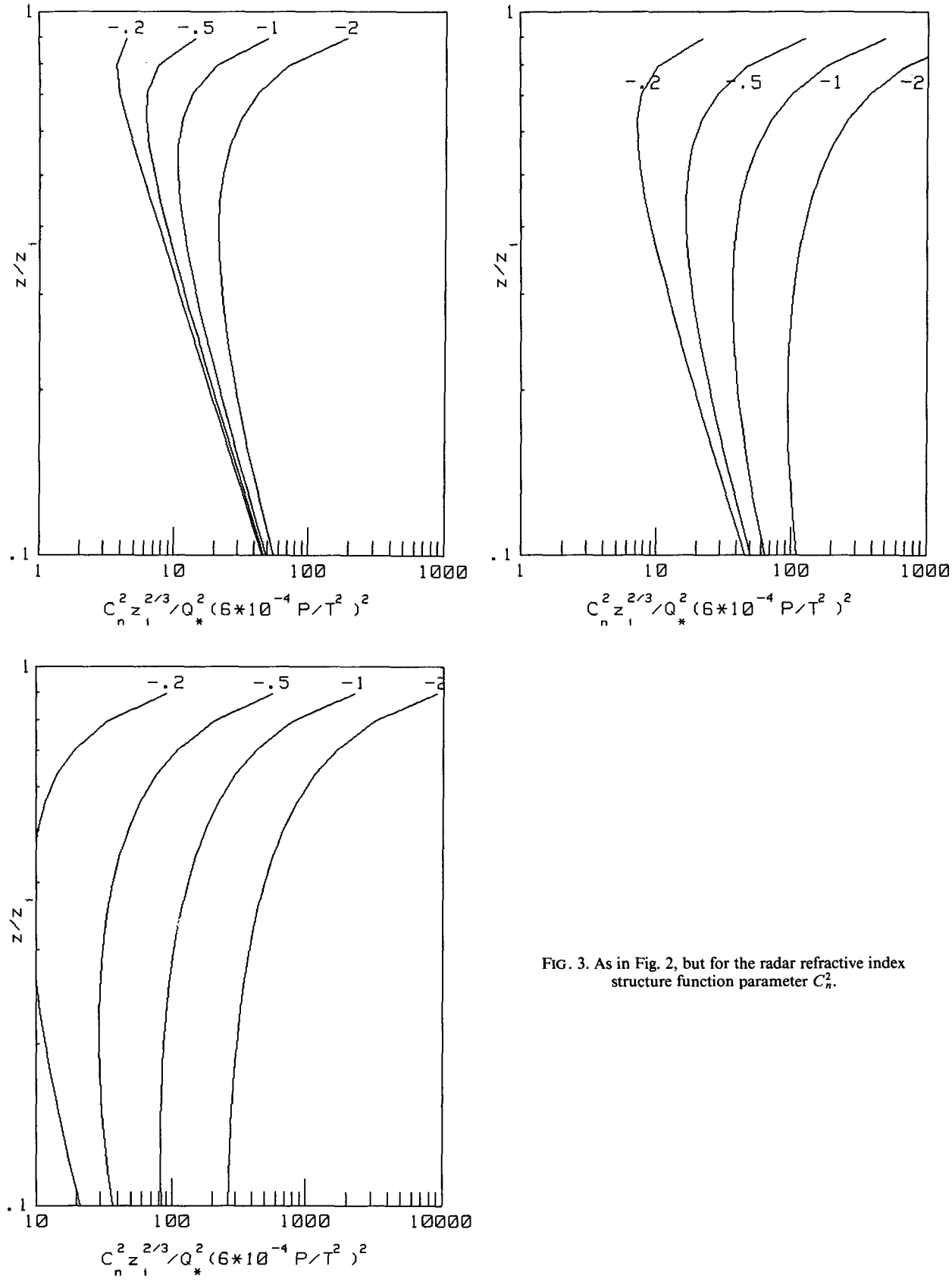

FIG. 3. As in Fig. 2, but for the radar refractive index structure function parameter C_n^2.

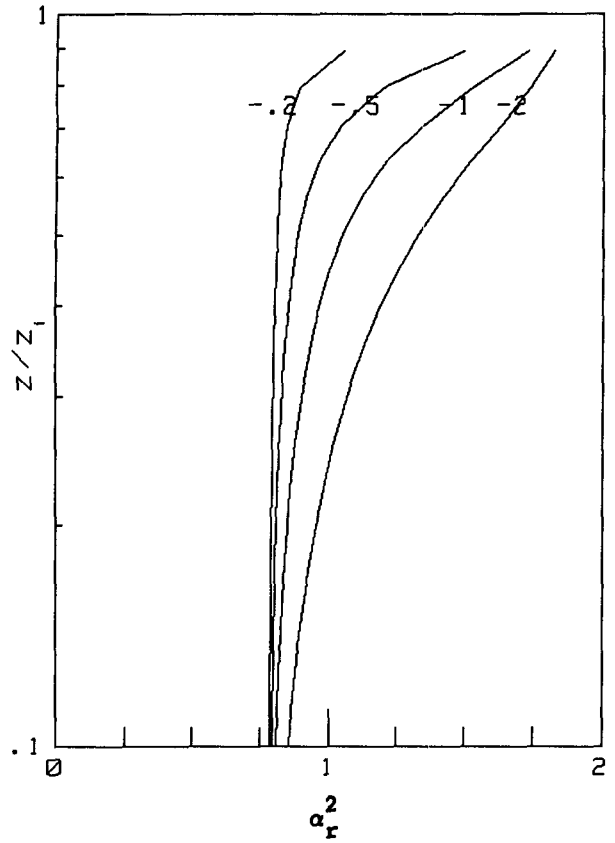

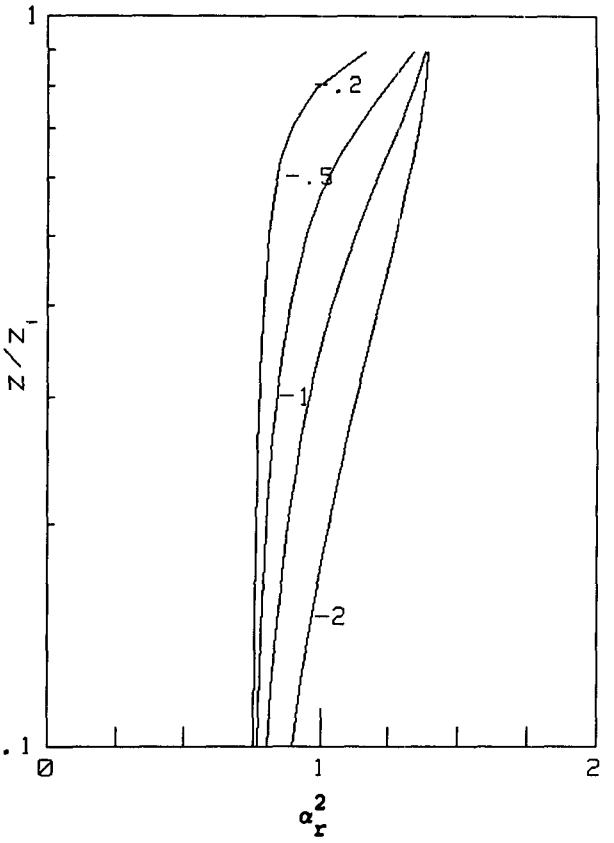

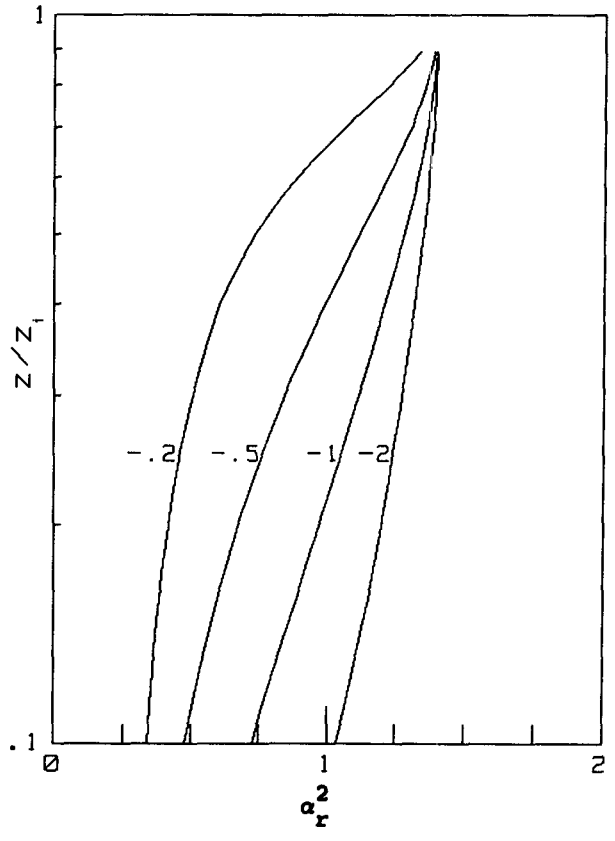

FIG. 4. As in Fig. 2, but for the pure moisture contribution parameter α_r^2.

ments (Fritschen and Qian 1990) over the Kansas prairie between June and October yielded noon values of β_0 between 0.2 and 8 with a typical value on the order of 0.5. This study will examine the profiles of variables r_{Tq}, C_n^2, and α_r^2 for these examples.

Profiles of r_{Tq} are shown in Fig. 2 for the three cases given in Table 2. These profiles show the increasing influence of entrainment as R_T and $-\beta_0/\beta_i$ increase. As was discussed in section 4, regions with r_{Tq} near zero probably have negligible temperature contributions to C_n^2. Figure 3 shows normalized C_n^2 profiles for the three cases. Note the change of scale for Fig. 3c. There are substantial differences between the marine and over land cases, but these are due more to entrainment-induced differences in $f_q(\xi)$ associated with β_0/β_i than in α_r^2. This is apparent in the profiles of α_r^2 given in Fig. 4. The large value of $-\beta_i$ in case one causes significant temperature effects near the top of the mixed layer in contrast to case 2. The overland case indicates substantial temperature effects throughout most of the boundary layer for the classic entrainment ratio $R_T = -0.2$, with moisture contributing only about 30% of C_n^2 in the lower half of the mixed layer. The moisture contribution increases substantially with increases in entrainment. Finally, in Fig. 5 the effect of the surface Bowen ratio is shown explicitly for the over land case with $R_T = -0.2$. Clearly the effects of β_0 are dramatic for $z/z_i < 0.5$, but only moderate in the upper half of the PBL.

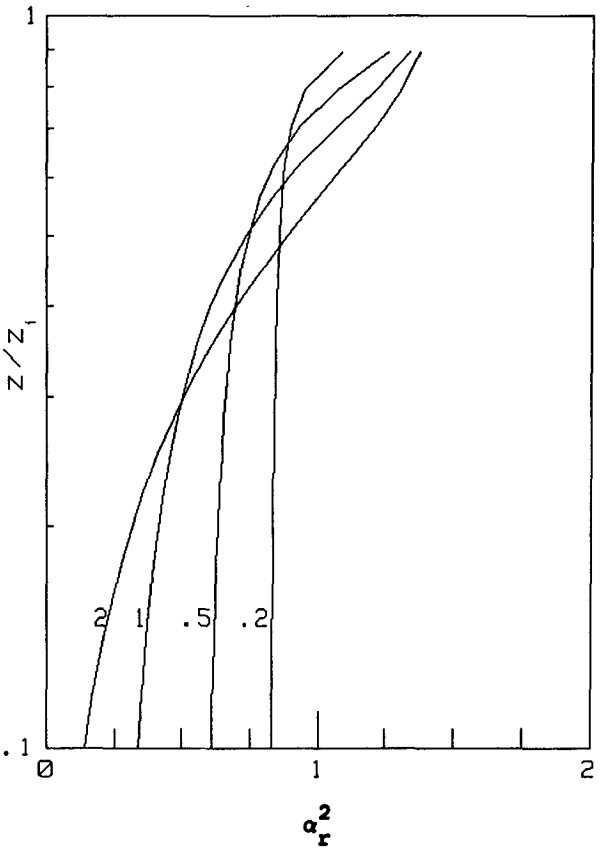

FIG. 5. Moisture contribution parameter α_r^2 versus the log of the normalized height for $R_{Tv} = -0.2$ and $\beta_i = -0.4$. The different curves correspond to different values of surface Bowen ratio β_0.

6. Discussion

On the basis of the model described in this paper, we can reach several conclusions regarding the cloud-free, convective PBL. In the lower part of the PBL, the structure function profiles tend to be determined by surface-layer similarity relationships based on the surface fluxes (Burk 1980). Typical values of β over the ocean are on the order of 0.1 to 0.5, but are as high as 2.0 in the Arctic: A value of 0.25 yields $\alpha_r^2 = 0.78$. Thus, the actual value of C_n^2 is on the order of 25% less than the pure moisture value for this case. In the upper parts of the boundary layer, entrainment and clouds play an important role in determining α_r^2. If $-\beta_i$ is less than about 0.5, then the errors will remain less than 25% throughout most of the PBL. This agrees with a series of 10 aircraft profiles of C_T^2 and C_q^2 made by Fairall (1982) off California and in the Bahamas (a summary of these measurements appeared in Fairall 1984) and also agrees with Burk's (1981) evaluation of α_r^2 in the inversion region. Over land surface Bowen ratios are often on the order of 1.0. Forests, active agricultural areas, swamps, etc., can easily have $\beta_0 < 0.5$; deserts can easily have $\beta_0 > 5$. Clearly, the assumption that radar measurements of C_n^2 are a surrogate for C_q^2 in the PBL over land must be backed up by direct measurements of β_0. Except in cases of unusually high values of $-\beta_i$, C_n^2 will also be a poor surrogate for C_T^2 in the over land PBL because of the entrained moisture effects near the top of the PBL.

The conclusions stated previously are based on a top-down/bottom-up diffusion model. The model is quite simple; the shape of the profiles being determined by only a few basic surface and inversion parameters. However, its application is restricted to convective conditions with a clearly established capping inversion and generally clear skies. The model is based on LES statistics and has been checked against several datasets, but a comprehensive study with clear-air radar, aircraft, and surface flux measurements has not been done.

Because the model is not directly applicable to the cloud-topped boundary layer, we cannot expect the details of this study to apply to that regime, but on simple physical reasoning we expect that the result for α_r^2 is roughly valid for the entrainment-induced effects associated with the clouds. This is also borne out by the second-order closure model study of Burk (1980), where moisture dominated radar C_n^2 for two MABL cases he examined, even in the presence of clouds. Clouds change the situation in the boundary layer in three ways: condensation processes create an additional thermodynamic coupling between temperature and

moisture, cloud-top longwave cooling greatly increases the rate of entrainment of warm, dry air from the free troposphere, and cloud and drizzle liquid-water droplets provide an additional scattering mechanism for the radar. In principle, the top-down/bottom-up approach can be extended to the cloud-topped PBL case by using conservative temperature and moisture variables (e.g., equivalent potential temperature and total moisture), as is done in second-order closure models (Burk 1980). Additional equations are required to convert from the conservative variable structure functions to the normal T and q variables we want to work with. Also, R_T will be strongly dependent on the longwave cooling at cloud top (for example, Stage and Businger 1981).

Acknowledgments. This work has been supported by the Office of Naval Research (Grant N00014-90-F-0027). The author wishes to thank Dr. Chin-Hoh Moeng for providing unpublished LES results.

REFERENCES

Balsley, B. B., and K. S. Gage, 1982: On the use of radars for operational wind profiling. *Bull. Amer. Meteor. Soc.*, **63,** 1009–1018.

Burk, S. D., 1980: Refractive index structure parameters: Time-dependent calculations using a numerical boundary-layer model. *J. Appl. Meteor.*, **19,** 562–576.

——, 1981: Temperature and humidity effects on refractive index fluctuations in upper regions of the convective boundary layer. *J. Appl. Meteor.*, **20,** 717–721.

Carlson, T. N., 1986: Regional-scale estimates of surface moisture availability and thermal inertia using remote thermal measurements. *Remote Sens. Rev.*, **1,** 197–247.

Chadwick, R. B., and E. E. Gossard, 1986: Radar probing and measurement of the planetary boundary layer. Part I: Scattering from refractive index irregularities. *Probing the Atmospheric Boundary Layer,* D. Lenschow, Ed., Amer. Meteor. Soc., 163–182.

Druilhet, A., J. P. Frangi, D. Guedalia and J. Fontan, 1983: Experimental studies of the turbulence structure parameters of the convective boundary layer. *J. Climate Appl. Meteor.*, **22,** 594–608.

Ecklund, W. L., D. A. Carter and B. B. Balsley, 1988: A UHF wind profiler for the boundary layer: Brief description and initial results. *J. Atmos. Oceanic Technol.*, **5,** 432–441.

Fairall, C. W., 1982: An analysis of the Wyngaard–LeMone model of refractive index and micrometeorological structure functions at the top of a turbulent mixed layer. Tech. Rep. NPS63-82-006CR, Naval Postgraduate School, Monterey, CA, 101 pp. [Copies can be obtained from C. Fairall, R/E/WP7, NOAA, 325 Broadway, Boulder, CO 80303.]

——, 1984: Wind shear enhancement of entrainment and refractive index structure parameter at the top of a turbulent mixed layer. *J. Atmos. Sci.*, **41,** 3472–3484.

——, 1987a: Similarity theories and microturbulence in the atmospheric mixed layer. *Dynamics of the Oceanic Surface Mixed Layer,* P. Muller and D. Henderson, Eds., University of Hawaii Publication, 265–290.

——, 1987b: A top-down and bottom-up diffusion model of C_T^2 and C_q^2 in the entraining convective boundary layer. *J. Atmos. Sci.*, **44,** 1009–1017.

Fritschen, L. J., and P. Qian: Energy balance components from six sites in a native prairie. *Proc. Symposium on FIFE,* Anaheim, Amer. Meteor. Soc., 37–41.

Gossard, E. E., 1990: Radar research on the atmospheric boundary layer. *Radar in Meteorology,* D. Atlas, Ed., Amer. Meteor. Soc., 477–527.

Hakkinen, S., and D. J. Cavalieri, 1989: A study of oceanic surface heat fluxes in the Greenland, Norwegian, and Barents Seas. *J. Geophys. Res.*, **94,** 6145–6158.

Hill, R. J., 1989: Implications of Monin–Obukhov similarity theory for scalar quantities. *J. Atmos. Sci.*, **46,** 2236–2244.

Hsiung, J., 1986: Mean surface energy fluxes over the global ocean. *J. Geophys. Res.*, **91,** 10 585–10 606.

Kohsiek, W., 1982: Measuring C_T^2, C_q^2, and C_{Tq} in the unstable surface layer and their relations to the vertical fluxes of heat and moisture. *Bound.-Layer Meteor.*, **24,** 89–107.

Lilly, D. K., 1968: Models of cloud-topped mixed layers under a strong inversion. *Quart. J. Roy. Meteor. Soc.*, **94,** 292–309.

Moeng, C.-H., and J. C. Wyngaard, 1984: Statistics of conservative scalars in the convective boundary layer. *J. Atmos. Sci.*, **41,** 3162–3169.

——, and J. C. Wyngaard, 1989: Evaluation of turbulent transport and dissipation closures in second-order modeling. *J. Atmos. Sci.*, **46,** 2311–2330.

Ottersten, H., 1969: Atmospheric structure and radar backscattering in clear air. *Radio Sci.*, **4,** 1179–1193.

Panofsky, H. A., and J. A. Dutton, 1984: *Atmospheric Turbulence.* John Wiley and Sons, 397 pp.

Prentice, K. C., 1990: Bioclimatic distribution of vegetation for general circulation model studies. *J. Geophys. Res.*, **95,** 11 811–11 830.

Priestly, C. H. B., and R. J. Taylor, 1972: On the assessment of surface heat flux and evaporation using large-scale parameters. *Mon. Wea. Rev.*, **100,** 81–92.

Priestley, J. T., and R. J. Hill, 1985: Measuring high-frequency humidity, temperature, and radio refractive index in the surface layer. *J. Atmos. Oceanic Technol.*, **2,** 233–251.

Rabadi, J. K. E., 1990: Surface-layer transfer processes over vegetation: A micrometeorological field experiment of long duration. Ph.D. thesis, Pennsylvania State University, University Park, PA, 161 pp.

Smith, S. D., 1988: Coefficients for sea surface wind stress, heat flux, and wind profiles as a function of wind speed and temperature. *J. Geophys. Res.*, **93,** 15 476–15 472.

Stage, S. A., and J. A. Businger, 1981: A model for entrainment into a cloud-topped marine boundary layer. Part I: Model description and application to a cold-air outbreak episode. *J. Atmos. Sci.*, **38,** 2213–2229.

Strauch, R. G., D. A. Merrit, K. P. Moran, K. B. Earnshaw and D. van de Kamp, 1984: The Colorado wind-profiling network. *J. Atmos. Oceanic Technol.*, **1,** 37–49.

Stull, R. B., 1988: *An Introduction to Boundary Layer Meteorology.* Kluwer Academic Publishers, 665 pp.

Tennekes, H., and A. G. M. Driedonks, 1981: Basic entrainment equations for the atmospheric boundary layer. *Bound.-Layer Meteor.*, **20,** 515–531.

Wesely, M. L., 1976: The combined effect of temperature and humidity fluctuations on refractive index. *J. Appl. Meteor.*, **15,** 43–49.

Wyngaard, J. C., 1990: Scalar fluxes in the planetary boundary layer—theory, modeling, and measurement. *Bound.-Layer Meteor.*, **50,** 49–75.

——, and M. A. LeMone, 1980: Behavior of the refractive index structure parameter in the entraining convective boundary layer. *J. Atmos. Sci.*, **37,** 1573–1585.

——, and R. A. Brost, 1984: Top-down and bottom-up diffusion of a scalar in the convective boundary layer. *J. Atmos. Sci.*, **41,** 102–112.

——, Y. Izumi and S. A. Collins, 1971: Behavior of the refractive index structure parameter near the ground. *J. Opt. Soc. Amer.*, **61,** 1646–1650.

——, W. T. Pennell, D. H. Lenschow and M. A. LeMone, 1978: The temperature–humidity covariance budget in the convective boundary layer. *J. Atmos. Sci.*, **35,** 47–58.